



# Biome changes and their inferred climatic drivers in northern and eastern continental Asia at selected times since 40 cal ka BP

Fang Tian<sup>1,2</sup> · Xianyong Cao<sup>1</sup> · Anne Dallmeyer<sup>2</sup> · Gerrit Lohmann<sup>3,4</sup> · Xu Zhang<sup>3</sup> · Jian Ni<sup>5</sup> · Andrei Andreev<sup>6,7</sup> · Patricia M. Anderson<sup>8</sup> · Anatoly V. Lozhkin<sup>9</sup> · Elena Bezrukova<sup>10,11</sup> · Natalia Rudaya<sup>7,11,12,13</sup> · Qinghai Xu<sup>14</sup> · Ulrike Herzschuh<sup>1,15,16</sup>

Received: 31 July 2017 / Accepted: 1 November 2017  
© Springer-Verlag GmbH Germany, part of Springer Nature 2017

## Abstract

Recent global warming is pronounced in high-latitude regions (e.g. northern Asia), and will cause the vegetation to change. Future vegetation trends (e.g. the “arctic greening”) will feed back into atmospheric circulation and the global climate system. Understanding the nature and causes of past vegetation changes is important for predicting the composition and distribution of future vegetation communities. Fossil pollen records from 468 sites in northern and eastern Asia were biomised at selected times between 40 cal ka BP and today. Biomes were also simulated using a climate-driven biome model and results from the two approaches compared in order to help understand the mechanisms behind the observed vegetation changes. The consistent biome results inferred by both approaches reveal that long-term and broad-scale vegetation patterns reflect global-to hemispheric-scale climate changes. Forest biomes increase around the beginning of the late deglaciation, become more widespread during the early and middle Holocene, and decrease in the late Holocene in fringe areas of the Asian Summer Monsoon. At the southern and southwestern margins of the taiga, forest increases in the early Holocene and shows notable species succession, which may have been caused by winter warming at ca. 7 cal ka BP. At the northeastern taiga margin (central Yakutia and northeastern Siberia), shrub expansion during the last deglaciation appears to prevent the permafrost from thawing and hinders the northward expansion of evergreen needle-leaved species until ca. 7 cal ka BP. The vegetation-climate disequilibrium during the early Holocene in the taiga-tundra transition zone suggests that projected climate warming will not cause a northward expansion of evergreen needle-leaved species.

**Keywords** Siberia · China · Northern Asia · Model-data comparison · Pollen · Permafrost · Vegetation-climate disequilibrium

## Introduction

Eastern, central, and northern Asia is covered by various biomes reflecting two major climatic gradients. Along the south-north temperature gradient, vegetation changes from tropical rainforest, to subtropical evergreen broadleaved forest, warm-temperate deciduous forest, temperate mixed

conifer-deciduous broadleaved forest, boreal conifer forest (taiga), and ultimately to arctic tundra. In the mid-latitude areas, the biomes also reflect an east–west moisture gradient, changing from forest to steppe and to desert (Alpat’ev et al. 1976; Hilbig 1995; Hou 2001; Fang et al. 2005). Forest-free areas are restricted to the cold end of the temperature gradient (e.g. arctic tundra in northern Siberia where mean annual temperature is lower than  $-6$  °C) and the arid end of the moisture gradient (e.g. steppe and desert in arid central Asia where mean annual precipitation is less than 400 and 200 mm, respectively). Hence, climate is assumed to be the dominant control of modern biomes and forest distribution at a continental scale in northern and eastern Asia (e.g. Alpat’ev et al. 1976; Fang et al. 2005; Tchebakova et al. 2009).

Communicated by F. Bittmann.

**Electronic supplementary material** The online version of this article (<https://doi.org/10.1007/s00334-017-0653-8>) contains supplementary material, which is available to authorized users.

✉ Fang Tian  
Fang.Tian@awi.de

Extended author information available on the last page of the article

A vegetation-climate disequilibrium may arise, however, if the effects of non-climatic factors (e.g. soil, fire) dominate, or biotic characteristics (e.g. biotic interactions) delay the temporal or spatial response of vegetation to a climate forcing (e.g. Normand et al. 2011; Svenning and Sandel 2013; Herzsuh et al. 2016). In permafrost areas, for example, the summer thaw-depth may influence the occurrence of a specific biome, particularly evergreen or deciduous needle-leaf forests (e.g. Tchebakova et al. 2009; Helbig et al. 2016; Herzsuh et al. 2016). Biome distribution can also be impacted by changes in wildfire regime (Abaimov and Sofronov 1996; Abaimov et al. 2002). Additionally, Herzsuh et al. (2016), based on pollen and other environmental data from northern regions of the Russian Far East, propose that interglacial vegetation (particularly the presence or absence of evergreen conifers) was influenced primarily by the environmental state of the preceding glaciation rather than the contemporaneous interglacial climate. They argue that the vegetation-climate disequilibrium is related to the combined effects of permafrost persistence, distant glacial refugia, and fire (Herzsuh et al. 2016). Accordingly, the spatial and temporal complexity of biome distributions may be strongly influenced by the interaction of the various driving forces and associated feedback mechanisms (Abaimov et al. 2002; Tchebakova et al. 2009; Rogers et al. 2015). The vegetation responses to future climate changes are likely to be characterised by feedback mechanisms that result in vegetation-climate disequilibrium at both leading and trailing edges of those changes, as represented, for example, by lags in migration and delayed local extinctions, respectively (Svenning and Sandel 2013).

Global warming of 0.6 °C during the 20th century, translates into amplified air temperature increases (Huang et al. 2015) in northern high latitudes (Miller et al. 2010) and arid regions (Huang et al. 2017), but the timing and strength of the vegetation responses in these remote areas is still poorly understood. For example, 20th century warming caused shrub expansion (“arctic greening”) in northern Siberia (Sturm et al. 2001; Frost and Epstein 2014), whereas forest cover was reduced in central Yakutia from 1982 to 2005 due to permafrost degradation (Lloyd et al. 2011). In the semi-arid forests of inner Asia, tree growth has declined since 1994 due to a temperature-induced reduction in effective moisture (Liu et al. 2013). However, an increase in vegetation cover occurred between 1991 and 2000 on the Loess Plateau, especially in hilly regions (belonging to the semi-arid region), mainly as a result of ecological restoration (Sun et al. 2015). The transition zones between forest and non-forest biomes, therefore, will likely continue to be sensitive to climate change and human impact. A better understanding of the potential responses of these biomes to future climate conditions can be gained by examining past

vegetation-climate relationships from palaeobotanical proxy data and computer models.

Broad-scale vegetation reconstructions have been undertaken that focus in part on eastern and northern Asia, including biomisation reconstruction (Ni et al. 2014; Tarasov et al. 1998, 2000; Bigelow et al. 2003; Binney et al. 2017), pollen data mapping (Cao et al. 2015), quantitative tree-cover reconstruction (Tian et al. 2016), and macrofossil data mapping (Binney et al. 2009). These previous studies provide valuable insights into the general pattern of vegetation changes. For example, during the last glacial-interglacial cycle, besides the temperature-driven south-north shift, the forest biomes extended north-westward after the last deglaciation (particularly during the Holocene) and shrank south-eastward in the late Holocene (precipitation-driven) at the margins of the Asian Summer Monsoon (Ni et al. 2014; Cao et al. 2015; Tian et al. 2016). In northern Siberia, the forest biomes shifted into the present tundra region during the early and middle Holocene, as revealed by macrofossil (Binney et al. 2009) and pollen-based vegetation reconstructions (Tarasov et al. 1998, 2000; Bigelow et al. 2003; Rudaya et al. 2016; Binney et al. 2017; Zhilich et al. 2017). However, these previous studies have either a restricted spatial extent (e.g. Bigelow et al. 2003; Binney et al. 2017) or temporal resolution (Tarasov et al. 1998, 2000; Bigelow et al. 2003). In addition, they only focus on documenting past vegetation changes, while the driving factors behind them have not been investigated.

Fossil pollen datasets (Cao et al. 2013) for both eastern and central Asia and Siberia (we use Siberia in its broadest sense in this study, i.e. Russia east of the Ural Mountains) have been compiled encompassing high-quality recent pollen data with standardised age-depth models. We reconstruct biomes using 468 fossil pollen records from eastern, central, and northern Asia for selected times between 40 cal ka BP (calibrated thousands of years before present) and today, and compare these pollen-based biomes with biomes simulated in a global climate model at selected time-slices (21, 14, 9, 6, 0 cal ka BP), to (1) characterise the biome changes in space and time and (2) assess the possible mechanisms responsible for the observed changes in past vegetation.

## Materials and methods

### Pollen dataset

Our dataset consists of 468 records (Fig. 1; all geographic locations mentioned in the text are presented in ESM Appendix 1). A fossil-pollen dataset from China and Mongolia (Cao et al. 2013; 271 pollen records) was expanded and now includes 297 records (222 of them have  $\geq 3$  dates). An additional 171 pollen records were collected

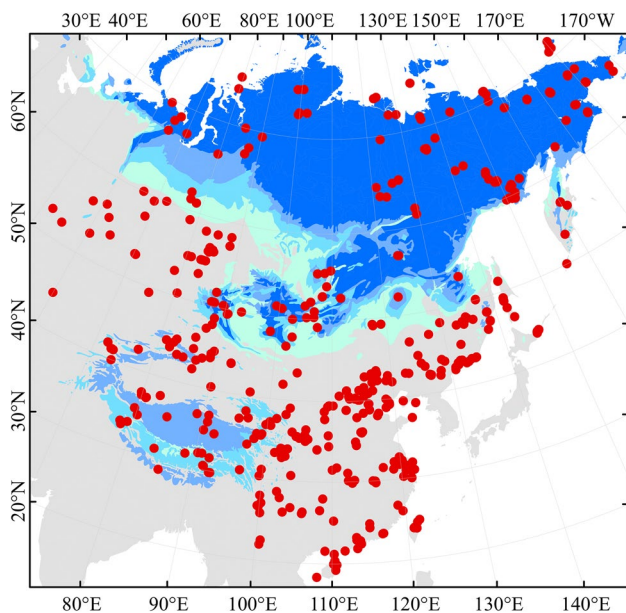


**Fig. 1** Fossil pollen sites from northern and eastern continental Asia used in this study

from northern Asia (mainly Siberia; north of 40°N and east of 50°E). Most of the northern pollen data (138 sites) were downloaded from open database sources (e.g. the Global Pollen Database, the European Pollen Database, Pangaea). We also included original counts contributed by their authors (17 sites) and digitised percentages from published pollen diagrams (16 sites). Only dated records were included in our analyses; most of the additional records (142 sites) have  $\geq 3$  radiocarbon dates. Age-depth relationships were established using Bayesian age-depth modelling (BACON routine implemented in R, Blaauw and Christen 2011). Pollen percentages were calculated based on the terrestrial pollen sum (excluding aquatic taxa but including Cyperaceae).

In previous biome-reconstruction approaches (e.g. Ni et al. 2014), a single time-nearest pollen sample was usually selected to represent the target time slice within a time window (time window = time slice  $\pm$  half span width), which may introduce high uncertainties because pollen percentages can vary from one level to the next. In this study, the mean value of taxa from all available pollen assemblages within a time window is selected as the “pollen sample” for a given time slice. For the middle and late Marine Isotope Stage 3 (MIS3) and the early last glacial maximum (LGM), the time slices are of 40, 35, 30, 27 and 25 cal ka BP with a half-span of 3,000 years for 40 cal ka BP and 2,000 years for the other time-slices. For the period between 22 and 12 cal ka BP, biomes are reconstructed at 1,000 year intervals with half-spans of 500 years for time slices between 22 and 16 cal ka BP and 200 years for 15–12 cal ka BP. In the Holocene,

24 time slices are selected between 11.5 and 0 cal ka BP at 500-year intervals with 150-year half-spans.

### Assignment of pollen taxa to biomes

Standard biomisation procedures to assign pollen taxa to plant functional types (PFTs) and then to biomes (Prentice et al. 1996; Prentice and Webb 1998) were employed for the 895 original pollen taxa in the 468 records through a global classification system of PFTs (Harrison et al. 2010). These followed the China biome reconstructions (Chen et al. 2010; Ni et al. 2010, 2014), with some minor changes in accordance with previous biome reconstructions for Siberia (Tarasov et al. 1998, 2000) and arctic high-latitude regions (Bigelow et al. 2003). The 895 pollen taxa were assigned to 80 PFTs, of which 51 PFTs were used to define 19 biomes (the anthropogenic biome in Ni et al. (2014) was not used; Table 1; ESM Appendix 2). In contrast to the Ni et al. (2014) assignment of PFTs to biomes, we assigned arctic-shrub PFTs (including erect/prostrate dwarf shrub, low and high shrub) to the biomes of boreal forests and tundra (Table 1). The PFT “bo.d.n.t.” (boreal deciduous needle-leaved tree, *Larix* spp.) is excluded from the four boreal forest biomes except for the cold deciduous forest biome (following Bigelow et al. 2003).

In the applied biomisation routine, pollen taxa with less than 0.5% abundance do not contribute to the calculation of the affinity score. We applied a weighting ( $\times 15$ ) to the pollen percentages of *Larix* prior to calculating the affinity score (following Bigelow et al. 2003 and Binney et al. 2017) to compensate for its low pollen production (Niemeyer et al. 2015). Bigelow et al. (2003) set this weighting because it resulted in the most realistic modern distribution of cold deciduous forest in Siberia.

A landscape openness index (Tarasov et al. 2013; Zhao et al. 2015) was calculated by subtracting the maximum forest biome score from the maximum non-forest biome score, to provide a qualitative assessment of changes in vegetation cover. A positive value indicates the dominance of non-forest biomes in the surroundings of the pollen site and increasing values indicate the landscape becoming more open.

### Climate modelling and biome simulations

To assess the potential bioclimatic drivers leading to the vegetation change in northern and eastern continental Asia, we compared the reconstructed vegetation with simulated biome distributions that are based on five time-slice simulations from a global climate model (21, 14, 9, 6, 0 ka BP). For this purpose, we used a consistent set of climate simulations generated from the comprehensive atmosphere-ocean-vegetation model COSMOS. Specific boundary conditions such as orbital parameters (Berger 1978) and land-surface

**Table 1** Assignment of plant functional types (PFTs) to biomes. A PFT in bold indicates a new addition to the PFT-Biome assignment in Ni et al. (2014) from referenced biome studies for northern Asia

(Tarasov et al. 1998, 2000; Bigelow et al. 2003). Text in brackets indicates PFTs excluded from the PFT-Biome assignment in Ni et al. (2014)

Biome code	Biome name	PFTs	Occurrence (5,734 in total)
CLDE	Cold deciduous forest	bo.cd.mb.t, bo.d.n.t, eu.e.n.t, bo.cd.mb.lhs, bo.e.mb.lhs, <b>ar.e.n.lhs, ar.e.mb.lhs, bo.e.n.lhs, ar.cd.mb.lhs, ar.e.mb.ed.s, ar.cd.mb.ed.s, ar.e.n.pds, ar.e.mb.pds, ar.cd.mb.pds</b>	339
CLEG	Cold evergreen needle-leaved forest	bo.cd.mb.t, bo.e.n.t, eu.e.n.t, bo.cd.mb.lhs, bo.e.mb.lhs, <b>ar.e.mb.lhs, ar.cd.mb.lhs, ar.e.mb.ed.s, ar.cd.mb.ed.s, ar.e.mb.pds, ar.cd.mb.pds (excluded bo.d.n.t)</b>	660
CLMX	Cold-temperate evergreen needle-leaved and mixed forest	bo.cd.mb.t, c-te.e.n.t, eu.e.n.t, bo.cd.mb.lhs, bo.e.mb.lhs (excluded bo.d.n.t)	329
COEG	Cool evergreen needle-leaved forest	bo.cd.mb.t, c-te.e.n.t, eu.e.n.t, te-ft.cd.mb.t, bo.cd.mb.lhs, bo.e.mb.lhs (excluded bo.d.n.t)	536
COMS	Cool mixed forest	c-te.e.n.t, eu.e.n.t, te-ft.cd.mb.t, te-fa.cd.mb.t, bo.e.mb.lhs, te.cd.mb.lhs (excluded bo.d.n.t)	267
TEDE	Temperate deciduous broad-leaved forest	bo.cd.mb.t, eu.e.n.t, te.e.n.t, te-fa.cd.mb.t, te-fi.cd.mb.t, te.cd.mb.lhs	180
WTEM	Warm-temperate evergreen broad-leaved and mixed forest	wt.e.mb.t, wt.e.n.t, wt.e.sb.t, wt.cd.mb.t, wt.d.n.t, te-fi.cd.mb.t, eu.e.n.t, wt.e.mb.lhs, wt.e.sb.lhs, wt.cd.mb.lhs	609
WTEG	Warm-temperate evergreen broad-leaved forest	wt.e.mb.t, wt.e.n.t, wt.e.sb.lhs, wt.e.sb.t, eu.e.n.t, wt.e.mb.lhs	0
TRSE	Tropical semi-evergreen broad-leaved forest	tr.e.mb.t, tr-m.dd.mb.t, wt.d.n.t, wt.e.mb.t, wt.e.n.t, wt.e.sb.t, tr.e.mb.lhs	16
TREG	Tropical evergreen broad-leaved forest	tr.e.mb.t, tr.e.sb.t, tu.t, wt.d.n.t, wt.e.mb.t, wt.e.n.t, wt.e.sb.t, tr.e.mb.lhs	5
TRDE	Tropical deciduous broad-leaved forest and woodland	tr-m.dd.mb.t, tr-x.dd.mb.t, tr-m.dd.mb.lhs, tr-x.dd.mb.lhs	0
TEXE	Temperate xerophytic shrubland	dt.sl.lhs, ml.t, sl.t, te-dt.fb	225
TEGR	Steppe	di.sl.lhs, eu-dt.fb, g, s, te-dt.fb	1,626
DESE	Desert	cs, dt.sl.lhs, ft.ml.lhs, g, ha, lsuc, ssuc	55
CUSH	Cushion-forb tundra	ar.fb, rc.fb	1
DRYT	Graminoid and forb tundra	ar.fb, g, s, <b>ar.e.mb.pds</b>	308
PROS	Prostrate dwarf shrub tundra	ar.cd.mb.pds, ar.e.mb.pds, ar.fb, <b>rc.fb, ar.e.n.pds</b>	96
DWAR	Erect dwarf shrub tundra	ar.cd.mb.ed.s, ar.cd.mb.pds, ar.e.mb.ed.s, ar.e.mb.pds, s, <b>ar.e.n.pds</b>	2
SHRU	Low and high shrub tundra	<i>ar.cd.mb.ed.s, ar.cd.mb.lhs, ar.cd.mb.pds, ar.e.mb.ed.s, ar.e.mb.lhs, ar.e.mb.pds, ar.e.n.lhs, ar.e.n.pds, g, s, bo.e.mb.lhs, bo.cd.mb.lhs, bo.e.n.lhs</i>	479

topography or greenhouse-gas concentrations were prescribed according to the PMIP3 protocol (<http://pmip3.lscce.ipsl.fr/>) and/or reconstructions for the different time slices. CO<sub>2</sub>-concentrations were set to 185 ppm for 21 ka BP, 240 ppm for 14 ka BP, 265 ppm for 9 ka BP, and 280 ppm for 6 and 0 ka BP. Further details on the model and climate simulations are described in ESM Appendix 3.

The simulated climate states have been used as forcing factors for the terrestrial biosphere model BIOME4 (Kaplan 2001; Kaplan et al. 2003) that calculates the equilibrium biome distribution for a prescribed climate, taking biogeographical and biogeochemical processes into account. Basic input variables are mean monthly temperature, cloud cover

(sunshine), precipitation, absolute minimum temperature, atmospheric CO<sub>2</sub>-concentration, and physical properties of soil such as water-holding capacity and percolation rates. BIOME4 distinguishes 28 different biomes that are further grouped into 12 mega-biomes in this study. The model has been slightly modified and recalibrated to better represent the regional biome distributions in eastern and northern Asia (Dallmeyer et al. 2017).

As a reference simulation for the pre-industrial biome distribution, BIOME4 has been forced with an atmospheric CO<sub>2</sub>-concentration of 280 ppm and the mean monthly climatology (1960–2000) of the University of East Anglia Climatic Research Unit Time Series 3.10 (CRU TS3.10,

University of East Anglia, 2008, Harris et al. 2014). Given the high spatial resolution ( $0.5^\circ \times 0.5^\circ$ ) of the CRU TS3.10 data, this dataset better resolves the complex climate gradients along the Asian orography and thus provides a more reliable climate background than pre-industrial climate reconstructions or simulations. A detailed discussion on the model performance and the reference simulation is given in Dallmeyer et al. (2017).

The biome distributions for the other time-slices have been calculated using an anomaly approach (Dallmeyer et al. 2017), i.e. the absolute differences between the mean monthly climatologies for each time-slice and the simulated pre-industrial climate have been added to the reference dataset. In the case of a negative value in the precipitation or cloudiness anomalies, these variables have been set to zero in the respective grid-boxes. The main advantage of the anomaly approach is the preservation of the regional, orography-induced climate pattern, although the complex Asian orography is not resolved at the coarse spatial resolution used in the climate model (Harrison et al. 1998). Furthermore, the influences of systematic climate biases on the biome distributions are minimised. Atmospheric  $\text{CO}_2$ -concentrations for other time slices (21, 14, 9, 6 cal ka BP) were set following the prescribed concentrations in the climate simulations. The absolute minimum temperature ( $T_{\min}$ ) was calculated from the mean temperature of the coldest month as described in Prentice et al. (1992).

To determine which climate variables are responsible for the biome shifts simulated by the model, we conducted a sensitivity study. Biome simulations were repeated for one time slice but we successively replaced the climate variables of the respective time-slice input data with one or more climate variables of the following time-slice. The biome differences between the modified run and original run should be caused by the changed climate variable. For instance, to test the sensitivity of biome distribution to precipitation change during the late Holocene (between 6 and 0 ka BP), we created an input dataset containing the 2 m-temperature, cloud cover, and absolute minimum temperature of the 6 ka data-set, but with the precipitation distribution of the CRU TS3.10 dataset for 0 ka BP (following Dallmeyer et al. 2017).

## Results

### General patterns of pollen-based biome reconstructions at a broad spatial scale

After the compilation of the original 21,682 fossil pollen samples from the 468 pollen records into 40 time windows, 5,734 pollen assemblages were obtained. The occurrence of each biome is presented in Table 1. The biomes tropical semi-evergreen broad-leaved forest (16 occurrences) and

tropical evergreen broad-leaved forest (5 occurrences) were combined into a new biome called tropical semi-evergreen/evergreen broad-leaved forest. The single occurrence of cushion-forb tundra was included in the biome graminoid and forb tundra (308 occurrences) and the biomes prostrate dwarf shrub tundra (96 occurrences) and erect dwarf shrub tundra (2 occurrences) were combined into the biome prostrate/erect dwarf shrub tundra (Table 1).

During the middle and late MIS 3 (represented by time slices 40, 35, 30, and 27 cal ka BP), forest biomes dominate only in the south-eastern parts of the study area and on the mid-latitude Pacific coast, while low and high shrub tundra and graminoid and forb tundra are broadly distributed across north-eastern Siberia. The inferred biome distribution for central Asia (including north-western China, south and south-western Mongolia, and northern Kazakhstan) is highly variable both temporally and spatially. Compared with late MIS3, steppe extends further east and dominates the landscape in north-central China (including the North China Plain, the Loess Plateau, and southern parts of the Mongolian Plateau) during the LGM (represented by time slices 25, 22, 21, and 20 cal ka BP). Furthermore, graminoid and forb tundra dominates the landscape in north-eastern Siberia, while low and high shrub tundra is reduced. During the last deglaciation (represented by time slices between 14 and 12 cal ka BP), forest biomes extend north-westward into the forest-steppe transition zone of China (north-central China), and low and high shrub tundra dominates all of Siberia. At the start of the Holocene, forest biomes are distributed throughout most of the study area except central Asia. Changes between forest- and non-forest biomes are strongest in the tundra-taiga transition zone in northern Siberia (Focus area 1), the forest-steppe transition zone in the southern West Siberian Plain and Baikal region (Focus area 2), and the forest-steppe transition zone in north-central China (Focus area 3). A more detailed description is provided for these three focus areas below.

### Focus area 1: biome transitions in the tundra-taiga transition zone in northern Siberia

During the middle and late MIS 3, low and high shrub tundra and graminoid and forb tundra dominate the landscape. Cold deciduous forest is reconstructed at one site near the southeastern coast (Olksy District). Low and high shrub tundra is replaced by graminoid and forb tundra during the LGM. During the last deglaciation, low and high shrub tundra dominates the landscape. From 13 cal ka BP, forest biome scores increase as reflected by the decrease in the landscape openness indices. At the beginning of the Holocene, cold deciduous forest appears in central Yakutia, and cold evergreen needle-leaved forest appears in the Olksy District and the Stanovoy Range. During the early Holocene, cold

deciduous forest and cold evergreen needle-leaved forest spread north and east, with cold deciduous forest becoming established along areas of the modern northern coast. The landscape is still open as revealed by the relatively high openness indices in the early Holocene, albeit less than at 0 ka. Cold evergreen needle-leaved forest establishes in central Yakutia at ca. 7 cal ka BP, associated with higher openness indices. Cold-temperate evergreen needle-leaved and mixed forest appears in central Yakutia at ca. 6.5 cal ka BP (Figs. 2, 3, ESM Appendices 4 and 5).

### **Focus area 2: biome transitions in the taiga-steppe transition zone of the southern West Siberian Plain and Baikal region**

During the middle and late MIS 3, evergreen needle-leaved forests occur as revealed by the only available site from the region. The few available pollen records indicate an open landscape during the last glacial period on the southern West Siberian Plain. From ca. 12 cal ka BP, forest biomes reappear, being a mixture of cold deciduous forest and cold evergreen needle-leaved forest, while the landscape is still open. From ca 7.5 cal ka BP, cold deciduous forests disappear, while cold-temperate evergreen needle-leaved and mixed forest and cool evergreen needle-leaved forest flourish within a forested landscape during the middle and late Holocene.

The landscape is also quite open before the Holocene in the Baikal region and the Altai Mountains. The Baikal region is covered by forest biomes throughout the Holocene, although the precise biome type changes notably. In the early Holocene (before ca. 6.5 cal ka BP), cold evergreen needle-leaved forest is the main biome with sporadic occurrence of cold deciduous forest, whereas during the late Holocene, cold-temperate evergreen needle-leaved and mixed forest becomes the main biome type, with cold evergreen needle-leaved forest as a subordinate biome. Cold evergreen needle-leaved forest appears in the Altai Mountains from 9.5 cal ka BP as the single biome type, indicating biome stability since the early Holocene (Figs. 2, 3, ESM Appendices 4, 5).

### **Focus area 3: forest-steppe transition zone in the fringe areas of the Asian summer monsoon**

Only one available site on the Loess Plateau covers the late MIS 3. It reveals forest biomes of cold evergreen needle-leaved forest or cold-temperate evergreen needle-leaved and mixed forest. During the LGM (from 22 to 17 cal ka BP), steppe is the dominant biome on the eastern Tibetan Plateau, the Loess Plateau, and in north-central China. During the last deglaciation, forest biomes, in particular cold and cool evergreen needle-leaved forests, re-appear. Forest biomes dominate during the early and middle Holocene (from 10.5 to ca. 4 cal ka BP). During the late Holocene, particularly

after ca. 2 cal ka BP, the areas of forest biome reduce and steppe increases with increasing landscape openness indices in north-central China and on the eastern Tibetan Plateau (Figs. 2, 3; ESM Appendices 4 and 5).

### **Model-based biome simulations, model-data comparison and inference of climate drivers for key time-slices (21, 14, 9, 6, 0 ka)**

The patterns of the model-estimated biome distributions for the five key time-slices are in general agreement with the pollen-based biome reconstructions (Fig. 4; ESM Appendix 6), although marked differences occur between some model-estimated and pollen-based biomes: (1) on the Tibetan Plateau—the tundra estimated by the model includes shrub tundra and steppe tundra mainly, while pollen-based results reveal steppe and forb tundra (we consider that the main compositions (e.g. Cyperaceae, Poaceae) are similar between these tundra and steppe types, hence we do not discuss the difference for the Tibetan Plateau); (2) in central Yakutia—a different extent of cold evergreen forest; and (3) in the forest-steppe transition zones in north-central and north-western China, southern and southwestern Mongolia, and northern Kazakhstan—different extent of steppe.

During the LGM (represented by the 21 ka time-slice), large parts of northern Asia (north of 60°N) are covered by tundra reflecting the generally cold and dry LGM climate (see ESM Appendix 7 for the climate for each of the five time slices). A belt of deciduous taiga is located between ca. 45°N and 60°N. Cold, temperate and warm forest biomes are restricted to south-eastern China, whereas grassland dominates north-central China, similar to the pollen-based results. The central Asian desert reaches far to the north (up to 65°N), which cannot currently be independently assessed because palynological data are not available from this region.

The biome distributions shift slightly between the LGM and the last deglaciation (represented by the 14 ka time-slice); the changes are generally consistent with the pollen-based results (ESM Appendix 6). Less precipitation (by up to 300 mm/year) on the Tibetan Plateau and in northeastern China may explain the expansion of the reconstructed desert biome in these regions at 14 ka. A sensitivity study (Fig. 5) reveals that the generally warmer climate (up to 4 °C) at 14 ka compared to the LGM leads to a replacement of ice-desert by tundra biomes in northeastern Siberia and along the northern coast. Grass and shrubland biomes slightly expand in western Siberia as growing degree days exceed the upper limits of boreal forest in the warmer climate. Furthermore, warm forest biomes spread northwards in southeastern China, induced by the post-LGM temperature increase (ESM Appendix 7).

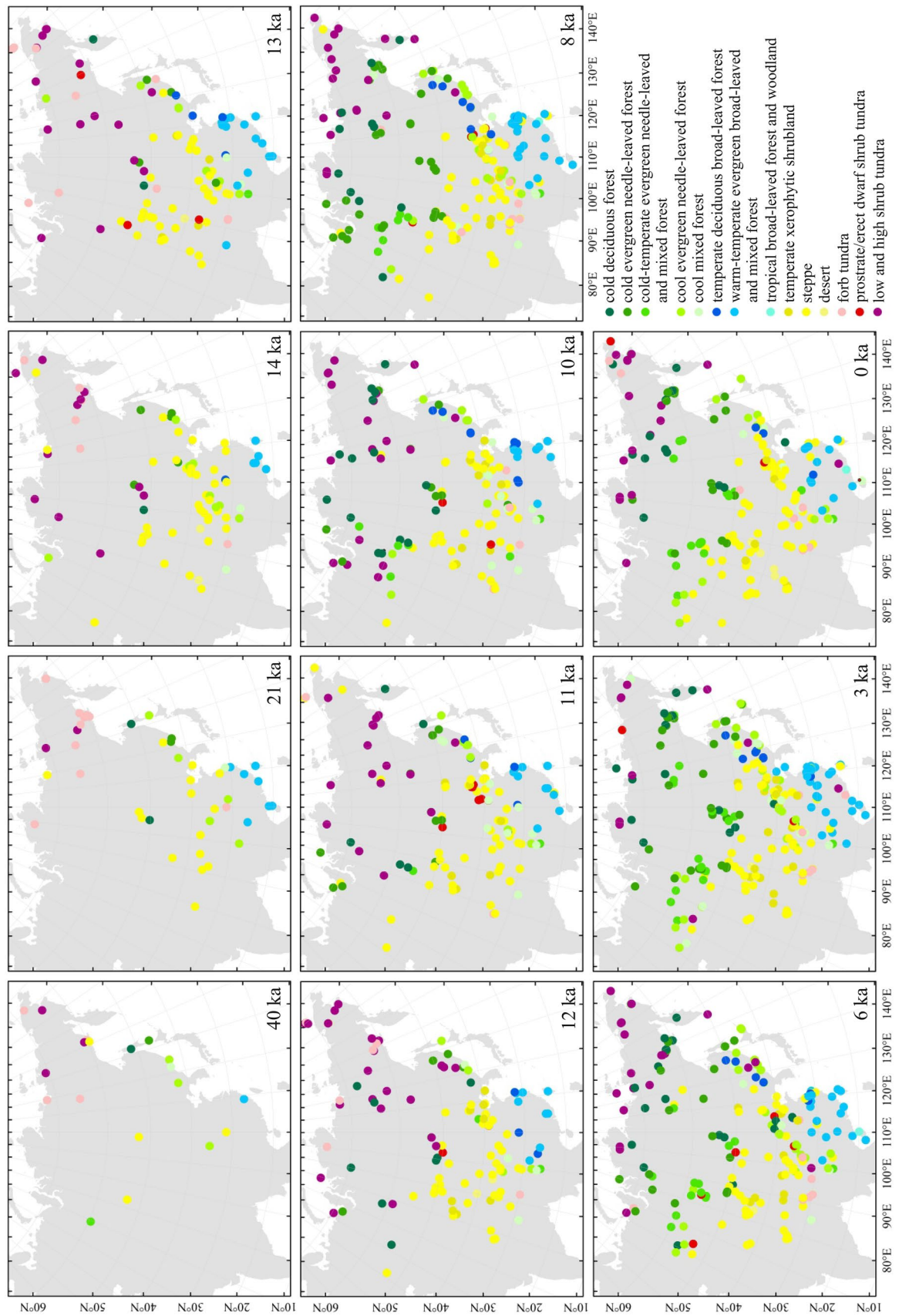


**Fig. 2** Pollen-based biome patterns at 11 key time slices since 40 cal ka BP (see ESM Appendix 4 for additional time slices)

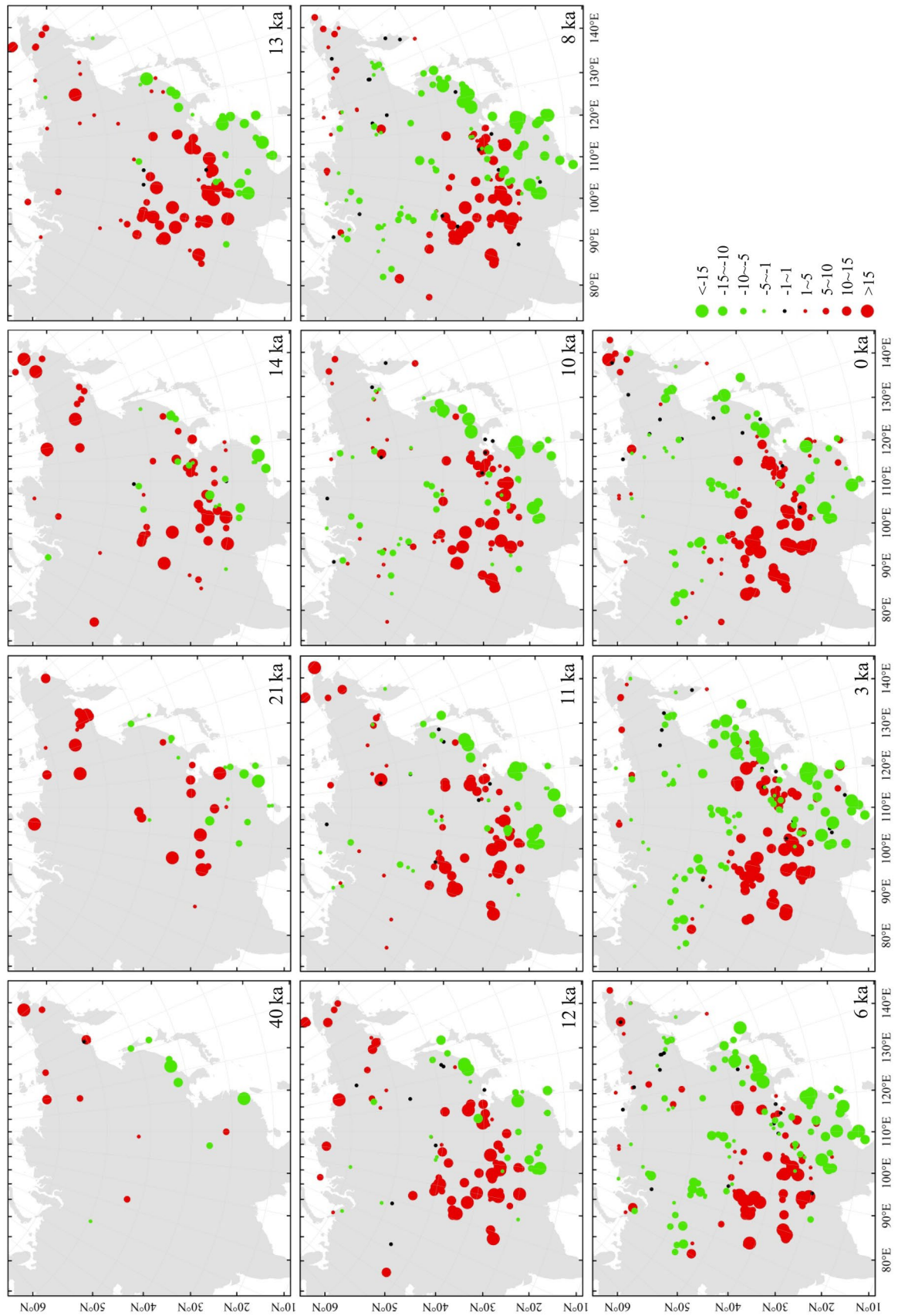




**Fig. 3** Openness distribution patterns at 11 key time slices since 40 cal ka BP (see ESM Appendix 5 for additional time slices). Openness is calculated by subtracting the maximum forest biome score from the maximum non-forest biome score (red=more open, green=more closed)

Deciduous taiga expands northwards and into the desert and shrubland regions in western Siberia. According to the sensitivity study, the slight northward expansion is related to the warmer climate at 14 ka as compared to the LGM. The replacement of desert/shrubland at this time can be related to either increased precipitation or an ecophysiological response to increased atmospheric CO<sub>2</sub>, because the water-use efficiency of plants is enhanced at higher CO<sub>2</sub> levels. The CO<sub>2</sub>-effect may also be responsible for the spread of temperate and cold forest biomes in eastern China and the appearance of evergreen taiga in northeastern China. The model results suggest that in Siberia as a whole, evergreen taiga is absent as winters are either too dry or too cold around 14 ka.

The distributions of the simulated biomes change markedly from the last deglaciation to the early Holocene (represented by the 9 ka time-slice), consistent with the pronounced climate change (ESM Appendix 7). Most striking is the broad-scale replacement of tundra biomes in northern Asia by forests. The sensitivity study suggests that the temperature increase is responsible for the tundra displacement only in southern Siberia and along the northwestern Siberian coast. In contrast, the widespread presence of forest in central Siberia, the southward expansion of cool/cold forest into the West Siberian Plain, and the vast spread of evergreen taiga can be explained by the joint effect of warmer climate plus increased precipitation. This tendency for forest biome reorganisation is supported by the pollen records, although too few records are available from most areas to resolve the biome transitions in great detail.

In line with the reconstructions, cool/cold forest biomes occur further north in the 9 ka simulation than at 14 ka, caused by increasing temperatures. More precipitation (up to 300 mm/year higher at 9 ka compared to 14 ka) results in a retreat of the desert area and an expansion of grassland and shrubland on the West Siberian Plain as well as a shift of the forest and steppe belt into the desert-steppe transition zone along the margins of the East Asian Monsoon. Furthermore, the model reveals a northward expansion of grasslands from north-central China into central Yakutia, which is hinted at in the site biomisations. According to the sensitivity study, this change originates from increased temperature in the southern part of the study area (i.e. the region around Lake Baikal) and from the joint effect of temperature and precipitation increases in the drier northern parts of south-central Yakutia.

Simulated vegetation changes only slightly from the early to middle Holocene (represented by the 6 ka time-slice), in

line with pollen results. The forest belts in Western Siberia retreat southward and are replaced by tundra along the northern coast. Taiga forest in central Yakutia expands at the expense of grassland. According to the sensitivity study, these changes could be exteriorly driven by decreasing temperatures (Figs. 4, 5).

During the late Holocene (from 6 to 0 ka), the cooling temperature of the boreal regions and associated reduction in growing degree days results in a southward shift of the taiga-tundra margin and the cool/cold forest biome in Western Siberia (Fig. 4). Furthermore, tundra replaces portions of the deciduous taiga in northeastern Siberia. Decreased precipitation related to a weaker East Asian Summer Monsoon at 0 ka leads to an increase in desert biome and an eastward retreat of shrubland and grassland and forests in north-central China.

Pollen-based reconstructions from central Yakutia show a high spatial and temporal heterogeneity, while the modelled results are more stable. Reconstructed biomes for this region mostly do not match the modelled biomes (Fig. 4; ESM Appendix 6).

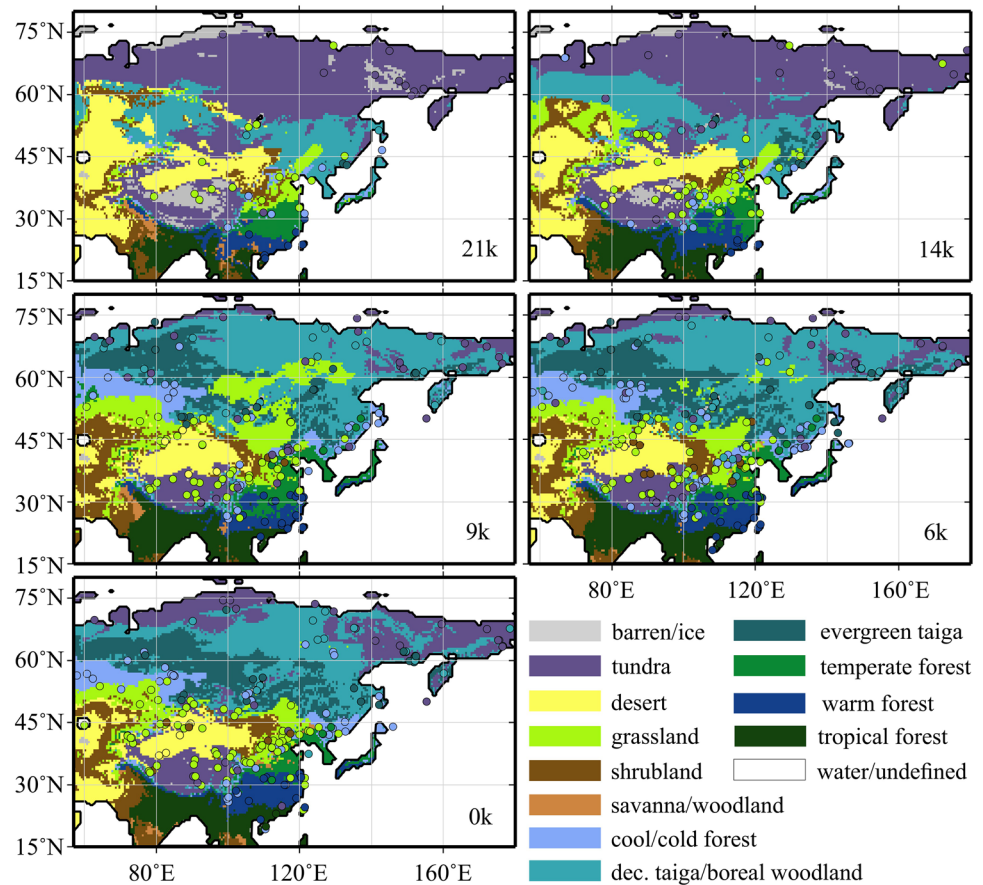
## Discussion

### Reliability of pollen-based biome reconstruction

We consider the biome reconstructions at the continental to sub-continental scale to be reliable. The pollen datasets used in this study have been carefully assessed and the assignment of pollen taxa to biomes is based on a widely accepted global classification system of plant functional types (PFTs) (Harrison et al. 2010) with some minor modifications (Tarasov et al. 1998, 2000; Bigelow et al. 2003; Ni et al. 2014; Binney et al. 2017). The results presented here are in agreement with previous biomisitation (e.g. Binney et al. 2017) and macrofossil studies (e.g. Binney et al. 2009). However, two aspects may limit the accuracy of the presented biome reconstructions and these can help explain the mismatch between the two biome reconstruction approaches.

1. Pollen taxa composition differs from the taxa composition in the vegetation of the source region in the study region as confirmed by regional studies of pollen productivity estimates (e.g. Wang and Herzschuh 2011; Xu et al. 2014; Niemeyer et al. 2015). In particular, *Larix* is strongly under-represented in the pollen spectra due to low productivity and poor dispersal and preservation (Niemeyer et al. 2015). Accordingly, a weight of  $\times 15$  was used for *Larix* (following Bigelow et al. 2003; Binney et al. 2017), while this issue was ignored for other taxa. The various pollen representations could be a major reason for the inconsistency between pollen-

**Fig. 4** The distribution of biomes simulated by BIOME4 at 21, 14, 9, 6, and 0 cal ka BP in comparison with pollen-based biomes



based and model-estimated biome results. For example, the over-estimated distribution of steppe in arid north-central China and central Asia may be a reflection of the over-representation of *Artemisia* and Chenopodiaceae pollen, and the over-estimated distribution of evergreen needle-leaved forests may likewise be a reflection of the over-representation of *Pinus* pollen (e.g. Liu et al. 1999; Xu et al. 2007) (Fig. 4).

- The taxonomic resolution may have affected the biome reconstruction results, particularly with respect to taxa that comprise both shrub and tree forms such as *Pinus*, *Alnus* and *Betula*, and could also to some extent cause a mismatch between pollen-based and simulated biomes. For example, in Siberia, the genus *Pinus* is represented by three major species with different life forms and from different bioclimatic zones: *Pinus sylvestris* (light taiga tree from the *Diploxylon* subgenus), *Pinus sibirica* (dark taiga tree from the *Haploxylon* subgenus), and *Pinus pumila* (north-east Asia high shrub species also from the *Haploxylon* subgenus) (Alvarez 1966; Tarasov et al. 1998; Tchebakova et al. 2009). While in most records *Pinus* pollen is separated into *Diploxylon* and *Haploxylon* subgenera, a separation between the shrub and tree forms of the *Haploxylon* subgenus is impossible. Such

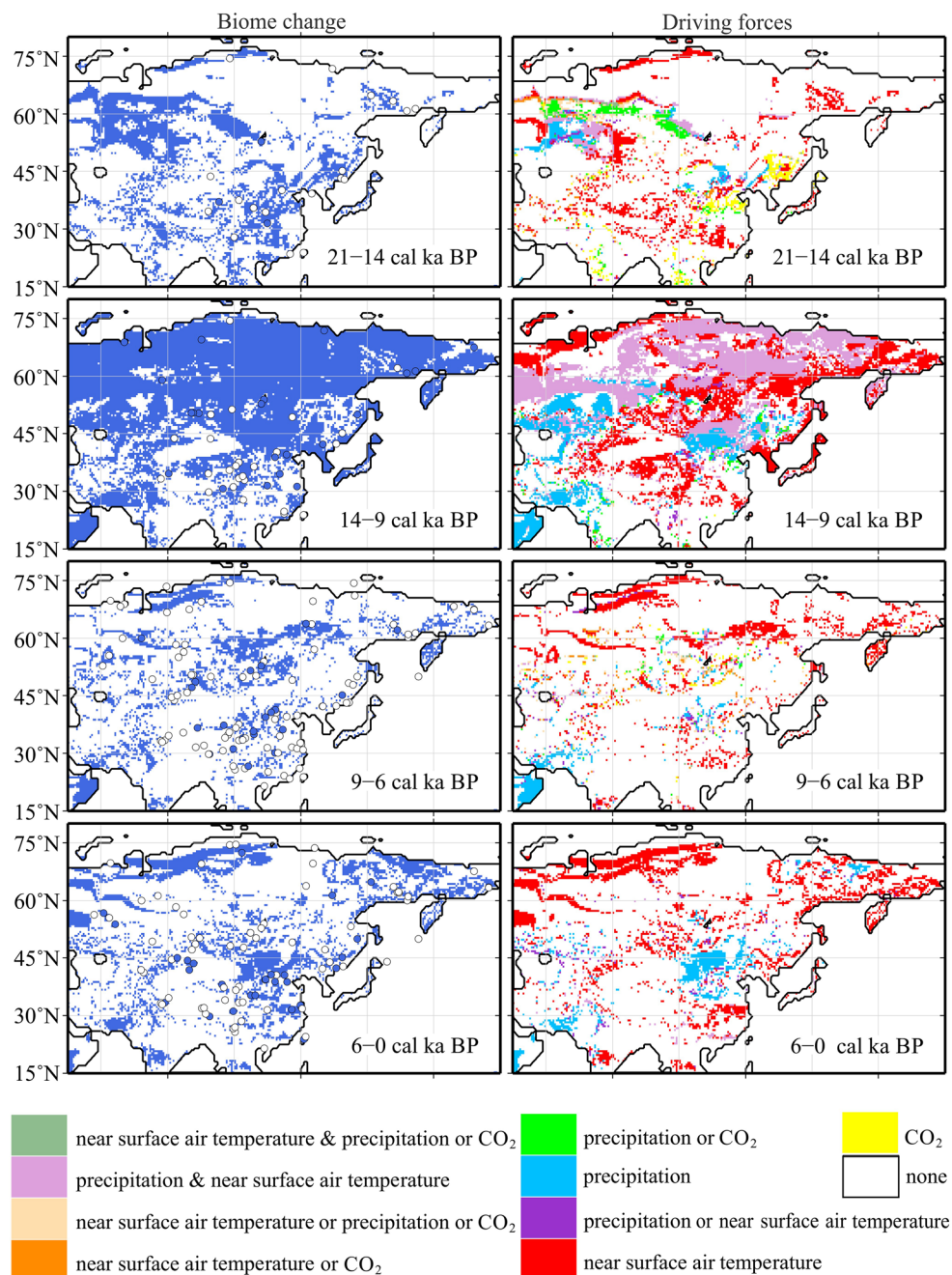
a taxonomic limitation for *Pinus* might explain the relatively widespread occurrence of evergreen conifer forest in northeastern Siberia as revealed by the pollen data.

### Potential driving forces of vegetation changes

The maps of the pollen-based biomes are generally consistent with the palaeovegetation patterns generated by the climate-model simulations (Fig. 6). This consistency at a continental to subcontinental scale indicates that climate is the most reasonable mechanism responsible for the biome shifts over the last 40 ka. Therefore, results from the climate sensitivity assessment should be particularly helpful in determining which climatic factors are primarily responsible for the past vegetation changes.

In the forest-steppe transition zone at lower latitudes (north-central China), the sensitivity tests indicate that precipitation is the primary driving force of vegetation change during the last glacial-interglacial cycle (Fig. 5). Increases in forest biomes, which began during the last deglaciation, are widespread during the early Holocene. These biome types are reduced and replaced by grassland during the late Holocene, possibly caused by the weakening of the summer

**Fig. 5** Biome changes between 21 and 14 cal ka BP, between 14 and 9 cal ka BP, between 9 and 6 cal ka BP, and between 6 and 0 cal ka BP (left panel, blue: grid-boxes with mega-biome transitions, white: no change within the time period). Right panel shows the climate factors responsible for the mega-biome changes according to a sensitivity study



monsoon (e.g. Cheng et al. 2016) as a result of the decline in summer solar insolation (Laskar et al. 2004) (Fig. 6).

In contrast, the sensitivity tests indicate that temperature is the main driving force in the tundra-taiga transition zone in northern Siberia over the last 40 ka, although these tests also indicate that precipitation plays an important role during the transition from the last deglaciation to the early Holocene (Fig. 5). Low and high shrub tundra dominates the landscape during the last deglaciation reflecting the relatively warmer climate, replacing the graminoid and forb tundra of the cold LGM. Temperature increases between the

last deglaciation and the early Holocene lead to a shift from ice-desert to tundra and from tundra to taiga in the north coast areas, while the widespread replacement of tundra by taiga in Siberia is explained by the joint effect of warmer climate (increases of up to 10 °C) and increased precipitation (increases of up to 400 mm) at 9 cal ka BP. The cooler climate at 0 cal ka BP induces the shift (only seen in the model) from taiga to tundra in northern Siberia and the Russian Far East during the late Holocene (Fig. 5).

Biome changes in the taiga-steppe transition zone on the southern West Siberian Plain (Fig. 5) are driven by various

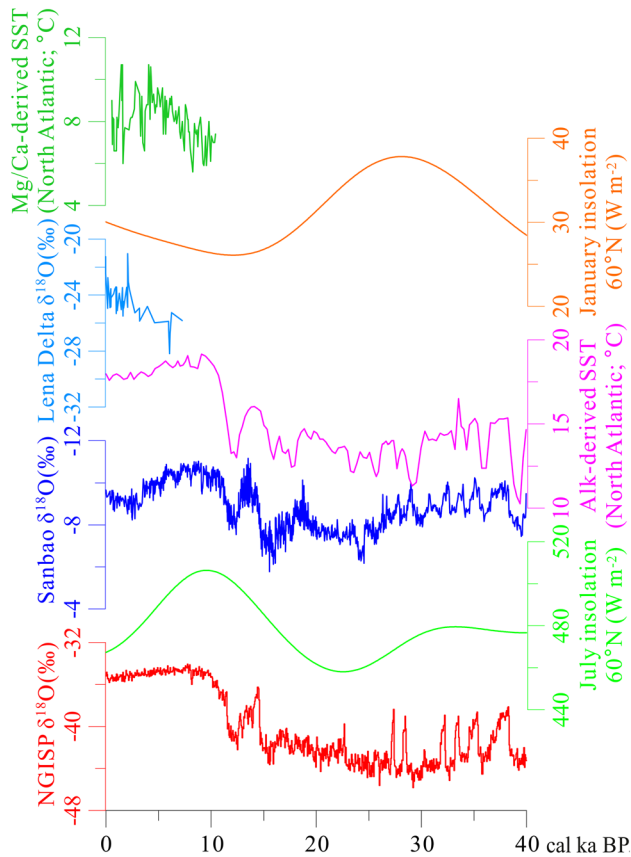


**Fig. 6** The proxy-based climate reconstructions from the Northern Hemisphere and solar insolation variations during the last 40 cal ka BP. NGRIP: the North Greenland Ice-Core Project (Andersen et al. 2004); Sanbao cave (Cheng et al. 2016); Alkenone-derived sea-surface temperature (SST) from deep-sea cores SU8118 and MD952042 (Pailler and Bard 2002); Mg/Ca-derived SST from core ODP-984 (Came et al. 2007); Lena Delta (Meyer et al. 2015); solar insolation in January and July at 60°N (Laskar et al. 2004)

forces. The expansion of deciduous taiga and the replacement of desert by temperate steppe and shrubland during the last deglaciation are likely caused by increased moisture availability to plants, either because of increased precipitation or an increase in  $\text{CO}_2$  which raises the water-use efficiency of plants (Morgan et al. 2004; Nelson et al. 2004).

### Possible reasons for a vegetation-climate disequilibrium

The mismatch between pollen-based and simulated biome results may, to some extent, be related to a vegetation-climate disequilibrium, particularly for the evergreen needle-leaved forest expansion after ca. 7 cal ka BP in central Yakutia.

Besides climate, permafrost is another important driver that can influence regional-scale vegetation changes in Siberia. For example, a comparison of ten terrestrial ecosystem

models, which exclude permafrost characteristics (Xia et al. 2017), indicates that net primary productivity in permafrost regions is overestimated by an average of 10% by the models in comparison with satellite-derived estimates.

Climate-vegetation-permafrost interactions are complex and, not surprisingly, are often poorly represented in Earth System models. Most vegetation models (including the one used in this study) do not include permafrost at all. Taking as an example the deciduous shrub biome expansion at ca. 13 cal ka BP in central Yakutia, the presence of the shrubs could have buffered the permafrost from the impact of climate warming and thus preserved the permafrost from thawing deeply (Herzschuh et al. 2016). Only shallow-rooting *Larix* forests could then invade such areas during the early Holocene, as indicated in the pollen-based biomisation. It is not until after about 7 cal ka BP that *Pinus* appears in the pollen records indicating that the active layer depth, at least in warm and sandy places and along riverbanks, was more than 1.5 m (Ermakov et al. 2002). In contrast, the modelling results indicate that due to a cooler climate and related lower evapotranspiration, deciduous taiga replaces grassland between 9 and 6 cal ka BP in central Yakutia.

In addition to climate and permafrost, wildfire is an important or even major ecological factor in controlling vegetation succession and biodiversity in Siberia (Abaimov and Sofronov 1996; Abaimov et al. 2002). Since ca. 7 cal ka BP, increased forest fire frequency (e.g. Shichi et al. 2009) has resulted in more open areas allowing the invasion of evergreen needle-leaved species into the cold deciduous forest.

## Conclusions

Pollen-based biome reconstructions for key time-slices for northern, central, and eastern Asia largely correspond to vegetation changes simulated by a BIOME4 model that has been linked with GCM scenarios. The major patterns include: (1) the dominance of non-forest vegetation during the LGM; (2) the expansion of forest or shrub biomes since the beginning of the last deglaciation (ca. 15 cal ka BP); (3) maximum forest expansion during the early and middle Holocene; and (4) forest retreat in northern Siberia and north-central China during the late Holocene. The similarity between vegetation reconstructed through biomisation of pollen records and that simulated by the climate model indicates that the palaeovegetation changes are driven primarily by climate changes (including atmospheric  $\text{CO}_2$ -concentration) at broad spatial and long temporal scales. The main climatic drivers can, however, produce notable regional differences. A mismatch between pollen-based and modelled biomes in central Yakutia during the Holocene probably originates from a vegetation-climate disequilibrium related to complex interactions between climate, permafrost, fire, and vegetation.

**Acknowledgements** The authors would like to express their gratitude to all the palynologists who, either directly or indirectly, contributed their pollen records to the pollen dataset. This research was supported by the German Research Foundation (DFG) and PalMod project (BMBF). Jian Ni was supported by the National Key Research and Development Program of China (2016YFC0502101). The work of Andrei Andreev was also partly performed under the Russian Government Program of Competitive Growth of Kazan Federal University. The work of Natalia Rudaya was founded by the Alexander von Humboldt Foundation (Ref 3.3-RUS-1151158-HFST-E); Ministry of Education and Science of the Russian Federation, Project no. 14.Z50.31.0010 of the Altai State University; Russian Government Program of Competitive Growth of Kazan Federal University; and the Russian Foundation for Basic Research (RFBR), Grant no. 16-55-44065. Additional support was provided to Anatoly Lozhkin by the Russian Foundation for Fundamental Research (15-05-06420) and Russian Academy of Sciences, Far East Branch (15-I-2-067). Cathy Jenks provided help with language editing.

## References

- Abaimov AP, Sofronov MA (1996) Main trends of past-fire successions in the near-tundra forests of Central Siberia. In: Goldammer JG, Furyaev VV (eds) *Fire in ecosystems of boreal Eurasia*. Kluwer Academic Publishers, Dordrecht, pp 372–386
- Abaimov AP, Zyryanova OA, Prokushkin SG (2002) Long-term investigations of larch forests in cryolithic zone of Siberia: brief history, recent results and possible changes under global warming. *Eurasian J Forest Res* 5:95–106
- Algreve KV (1966) Forest economy in the U.S.S.R.: An analysis of Soviet competitive potentialities. *Studia Forestalia Suecica* 39. Skogshögskolan, Stockholm
- Alpat'ev AM, Arkhangel'skii AM, Podoplelov NY, Stepanov AY (1976) *Fizicheskaya geografiya SSSR (Aziatskaya chast')*. Vysshaya Shkola, Moscow
- Andersen KK, Azuma N, Barnola JM et al (2004) High resolution record of Northern Hemisphere climate extending into the last interglacial period. *Nature* 431:147–151
- Berger A (1978) Long-term variations of daily insolation and Quaternary climate changes. *J Atmos Sci* 35:2,362–2,367
- Bigelow NH, Brubaker LB, Edwards ME et al (2003) Climate change and arctic ecosystems: 1. Vegetation changes north of 55°N between the last glacial maximum, mid-Holocene, and present. *J Geophys Res* 108:8170. <https://doi.org/10.1029/2002JD002558>
- Binney H, Edwards M, Macias-Fauria M et al V (2017) Vegetation of Eurasia from the last glacial maximum to present: key biogeographic patterns. *Quat Sci Rev* 157:80–97
- Binney HA, Willis KJ, Edwards ME et al (2009) The distribution of late-Quaternary woody taxa in northern Eurasia: evidence from a new macrofossil database. *Quat Sci Rev* 28:2,445–2,464
- Blaauw M, Christen JA (2011) Flexible paleoclimate age-depth models using an autoregressive gamma process. *Bayesian Anal* 6:457–474
- Came RE, Oppo DW, McManus JF (2007) Amplitude and timing of temperature and salinity variability in the subtropical North Atlantic over the last 10,000 years. *Geology* 35:315–318
- Cao X, Herzschuh U, Ni J, Zhao Y, Böhrer T (2015) Spatial and temporal distributions of major tree taxa in eastern continental Asia during the last 22,000 years. *Holocene* 25:79–91
- Cao X, Ni J, Herzschuh U, Wang Y, Zhao Y (2013) A late Quaternary pollen dataset from eastern continental Asia for vegetation and climate reconstructions: set up and evaluation. *Rev Palaeobot Palynol* 194:21–37
- Chen Y, Ni J, Herzschuh U (2010) Quantifying modern biomes based on surface pollen data in China. *Glob Planet Chang* 74:114–131
- Cheng H, Edwards RL, Sinha A et al (2016) The Asian monsoon over the past 640,000 years and ice age terminations. *Nature* 534:640–646
- Dallmeyer A, Claussen M, Ni J et al (2017) Biome changes in Asia since the mid-Holocene—an analysis of different transient Earth system model simulations. *Clim Past* 13:107–134
- Ermakov N, Cherosov M, Gogoleva P (2002) Classification of ultracontinental boreal forests in central Yakutia. *Folia Geobot* 37:419–440
- Fang J, Piao S, Zhou L, He J, Wei F, Myneni RB, Tucker CJ, Tan K (2005) Precipitation patterns alter growth of temperature vegetation. *Geophys Res Lett* 32:411–415
- Frost GV, Epstein HE (2014) Tall shrub and tree expansion in Siberian tundra ecotones since the 1960s. *Glob Chang Biol* 20:1,264–1,277
- Harris I, Jones PD, Osborn TJ, Lister DH (2014) Updated high-resolution grids of monthly climatic observations—the CRU TS3.10 dataset. *Int J Climatol* 34:623–642
- Harrison SP, Jolly D, Laarif F et al (1998) Intercomparison of simulated global vegetation distribution in response to 6 kyr BP orbital forcing. *J Clim* 11:2,721–2,742
- Harrison SP, Prentice IC, Barboni D, Kohfeld K, Ni J, Sutra JP (2010) Ecophysiological and bioclimatic foundations for a global plant functional classification. *J Veg Sci* 21:300–317
- Helbig M, Pappas C, Sonnentag O (2016) Permafrost thaw and wildfire: Equally important drivers of boreal tree cover changes in the Taiga Plains, Canada. *Geophys Res Lett* 43:1,598–1,606
- Herzschuh U, Birks HJB, Laepple T, Andreev A, Melles M, Brigham-Grette J (2016) Glacial legacies on interglacial vegetation at the Pliocene–Pleistocene transition in NE Asia. *Nat Commun* 11967. <https://doi.org/10.1038/ncomms11967>
- Hilbig W (1995) *The vegetation of Mongolia*. SPB Academic Publishing, Amsterdam
- Hou X (2001) *Vegetation Atlas of China*. Science Press, Beijing
- Huang J, Yu H, Dai A, Wei Y, Kang L (2017) Drylands face potential threat under 2 °C global warming target. *Nat Clim Chang* 7:412–422. <https://doi.org/10.1038/nclimate3275>
- Huang J, Yu H, Guan X, Wang G, Guo R (2015) Accelerated dryland expansion under climate change. *Nat Clim Chang* 6:166–171. <https://doi.org/10.1038/nclimate2837>
- Kaplan JO (2001) *Geophysical applications of vegetation modeling*. PhD Dissertation, Lund University, Lund
- Kaplan JO, Bigelow NH, Prentice IC et al (2003) Climate change and arctic ecosystems: 2. Modeling, paleodata-model comparisons, and future projections. *J Geophys Res* 108:8171. <https://doi.org/10.1029/2002JD002559>
- Laskar J, Robutel P, Joutel F, Gastineau M, Correia ACM, Levrard B (2004) A long-term numerical solution for the insolation quantities of the Earth. *Astron Astrophys* 428:261–285
- Liu H, Cui H, Pott R, Speier M (1999) The surface pollen of the woodland-steppe ecotone in southeastern Inner Mongolia, China. *Rev Palaeobot Palynol* 105:237–250
- Liu H, Williams AP, Allen C et al (2013) Rapid warming accelerates tree growth decline in semi-arid forests of Inner Asia. *Glob Chang Biol* 19:2,500–2,510
- Lloyd AH, Bunn AG, Berner L (2011) A latitudinal gradient in tree growth response to climate warming in the Siberian taiga. *Glob Chang Biol* 17:1,935–1,945
- Meyer H, Opel T, Laepple T, Dereviagin AY, Hoffmann K, Werner M (2015) Long-term winter warming trend in the Siberian Arctic during the mid- to late Holocene. *Nat Geosci* 8:122–125
- Miller GH, Alley R, Brigham-Grette J, Fitzpatrick JJ, Polyak L, Serreze MC, White JWC (2010) Arctic amplification: can the past constrain the future?. *Quat Sci Rev* 29:1,779–1,790
- Morgan JA, Pataki DE, Körner C et al (2004) Water relations in grassland and desert ecosystems exposed to elevated atmospheric CO<sub>2</sub>. *Oecologia* 140:11–25

- Nelson JA, Morgan JA, LeCain DR, Mosier AR, Milchunas DG, Parton WJ (2004) Elevated CO<sub>2</sub> increases soil moisture and enhances plant water relations in a long-term field study in the semi-arid shortgrass steppe of Northern Colorado. *Plant Soil* 259:169–179
- Ni J, Cao X, Jeltsch F, Herzschuh U (2014) Biome distribution over the last 22,000 year in China. *Palaeogeogr Palaeoclimatol Palaeoecol* 409:33–47
- Ni J, Yu G, Harrison SP, Prentice IC (2010) Palaeovegetation in China during the late Quaternary: biome reconstructions based on a global scheme of plant functional types. *Palaeogeogr Palaeoclimatol Palaeoecol* 289:44–61
- Niemeyer B, Klemm J, Pestryakova LA, Herzschuh U (2015) Relative pollen productivity estimates for common taxa of the northern Siberian Arctic. *Rev Palaeobot Palynol* 221:71–82
- Normand S, Ricklefs RE, Skov F, Bladt J, Tackenberg O, Svenning JC (2011) Postglacial migration supplements climate in determining plant species ranges in Europe. *Proc Royal Soc B: Biol Sci* 278:2,644–2,653. <https://doi.org/10.1098/rspb.2010.2769>
- Pailler D, Bard E (2002) High frequency paleoceanographic changes during the past 140,000 years recorded by the organic matter in sediments off the Iberian Margin. *Palaeogeogr Palaeoclimatol Palaeoecol* 181: 431–452
- Prentice IC, Cramer W, Harrison SP, Leemans R, Monserud RA, Solomon AM (1992) A global biome model based on plant physiology and dominance, soil properties and climate. *J Biogeogr* 19:117–134
- Prentice IC, Guiot J, Huntley B, Jolly D, Cheddadi R (1996) Reconstructing biomes from palaeoecological data: a general method and its application to European pollen data at 0 and 6 ka. *Clim Dyn* 12:185–194
- Prentice IC, Webb III T (1998) BIOME 6,000: reconstructing global mid-Holocene vegetation patterns from palaeoecological records. *J Biogeogr* 25:997–1,005
- Rogers BM, Soja AJ, Goulden ML, Randerson JT (2015) Influence of tree species on continental differences in boreal fires and climate feedbacks. *Nat Geosci* 8:228–234
- Rudaya N, Nazarova L, Novenko E et al (2016) Quantitative reconstructions of mid-late Holocene climate and vegetation in the north-eastern Altai Mountains recorded in Lake Teletskoye. *Glob Planet Chang* 141:12–24
- Shichi K, Takahara H, Krivonogov SK, Bezrukova EV, Kashiwaya K, Takehara A, Nakamura T (2009) Late Pleistocene and Holocene vegetation and climate records from Lake Kotokel, central Baikal region. *Quat Int* 205:98–110
- Sturm M, McFadden J, Liston G (2001) Snow-shrub interactions in Arctic tundra: a hypothesis with climatic implications. *J Clim* 14:336–344
- Sun W, Song X, Mu X, Gao P, Wang F, Zhao G (2015) Spatiotemporal vegetation cover variations associated with climate change and ecological restoration in the Loess Plateau. *Agric For Meteorol* 209–210:87–99
- Svenning JC, Sandel B (2013) Disequilibrium vegetation dynamics under future climate change. *Am J Bot* 100:1,266–1,286
- Tarasov PE, Andreev AA, Anderson PM et al (2013) A pollen-based biome reconstruction over the last 3.562 million years in the Far East Russian Arctic—new insights into climate-vegetation relationships at the regional scale. *Clim Past* 9:2,759–2,775
- Tarasov PE, Volkova VS, Webb T III et al (2000) Last glacial maximum biomes reconstructed from pollen and plant macrofossil data from northern Eurasia. *J Biogeogr* 27:609–620
- Tarasov PE, Webb T III, Andreev AA et al (1998) Present-day and mid-Holocene biomes reconstructed from pollen and plant macrofossil data from the Former Soviet Union and Mongolia. *J Biogeogr* 25:1,029–1,053
- Tchekakova NM, Parfenova E, Soja AJ (2009) The effects of climate, permafrost and fire on vegetation change in Siberia in a changing climate. *Environ Res Lett* 4:045,013
- Tian F, Cao X, Dallmeyer A, Ni J, Zhao Y, Wang Y, Herzschuh U (2016) Quantitative woody cover reconstructions from eastern continental Asia of the last 22 ka reveal strong regional peculiarities. *Quat Sci Rev* 137:33–44
- Wang Y, Herzschuh U (2011) Reassessment of Holocene vegetation change on the upper Tibetan Plateau using the pollen-based REVEALS model. *Rev Palaeobot Palynol* 168:31–40
- Xia J, McGuire AD, Lawrence D et al (2017) Terrestrial ecosystem model performance in simulating productivity and its vulnerability to climate change in the northern permafrost region. *J Geophys Res Biogeosciences* 122:430–446
- Xu QH, Cao X, Tian F, Zhang SR, Li YC, Li M, Liu Y, Liang J (2014) Relative pollen productivities of typical steppe species in northern China and their potential in past vegetation reconstruction. *Sci China Earth Sci* 57:1,254–1,266
- Xu QH, Li YC, Yang XL, Zheng ZH (2007) Quantitative relationship between pollen and vegetation in northern China. *Sci China Series D Earth Sci* 50:582–599
- Zhao WW, Andreev AA, Wennrich V, Tarasov PE, Anderson P, Lozhkin AV, Melles M (2015) The Réunion Subchron vegetation and climate history of the northeastern Russian Arctic inferred from the Lake El'gygytgyn pollen record. *Palaeogeogr Palaeoclimatol Palaeoecol* 436:167–177
- Zhilich S, Rudaya N, Nazarova L, Krivonogov S, Pozdnyakov D (2017) Environmental dynamics of the Baraba forest-steppe (Siberia) over the last 8000 years and their impact on the types of economic life of the population. *Quat Sci Rev* 163:152–161

## Affiliations

Fang Tian<sup>1,2</sup> · Xianyong Cao<sup>1</sup> · Anne Dallmeyer<sup>2</sup> · Gerrit Lohmann<sup>3,4</sup> · Xu Zhang<sup>3</sup> · Jian Ni<sup>5</sup> · Andrei Andreev<sup>6,7</sup> · Patricia M. Anderson<sup>8</sup> · Anatoly V. Lozhkin<sup>9</sup> · Elena Bezrukova<sup>10,11</sup> · Natalia Rudaya<sup>7,11,12,13</sup> · Qinghai Xu<sup>14</sup> · Ulrike Herzschuh<sup>1,15,16</sup>

<sup>1</sup> Research Unit Potsdam, Alfred Wegener Institute, Helmholtz Centre for Polar and Marine Research, Telegrafenberg A43, 14473 Potsdam, Germany

<sup>2</sup> Max Planck Institute for Meteorology, KlimaCampus, Bundesstraße 53, 20146 Hamburg, Germany

<sup>3</sup> Alfred Wegener Institute, Helmholtz Centre for Polar and Marine Research, Am Handelshafen 12, 27570 Bremerhaven, Germany

<sup>4</sup> MARUM-Center for Marine Environmental Sciences, University of Bremen, Leobener Straße 8, 28359 Bremen, Germany

<sup>5</sup> College of Chemistry and Life Sciences, Zhejiang Normal University, Yingbin Avenue 688, Jinhua 321004, China

<sup>6</sup> Institute of Geology and Mineralogy, University of Cologne, Zùlpicher Straße 49a, 50674 Cologne, Germany

- <sup>7</sup> Institute of Geology and Petroleum Technologies, Kazan Federal University, Kazan 420008, Russia
- <sup>8</sup> Earth and Space Sciences and Quaternary Research Center, University of Washington, Seattle, WA 98185, USA
- <sup>9</sup> North East Interdisciplinary Science Research Institute, Far East Branch Russian Academy of Sciences, Magadan 685000, Russia
- <sup>10</sup> Vinogradov Institute of Geochemistry, Siberian Branch, Russian Academy of Sciences, ul. Favorskogo 1a, Irkutsk 664033, Russia
- <sup>11</sup> Institute of Archaeology and Ethnography, Siberian Branch, Russian Academy of Sciences, pr. Akad. Lavrentieva 17, Novosibirsk 630090, Russia
- <sup>12</sup> Department of Archaeology and Ethnography, Novosibirsk State University, Pirogova 2, Novosibirsk 630090, Russia
- <sup>13</sup> Department of Archaeology and Ethnography, Altai State University, Str. Lenina, 61, Barnaul 656049, Russia
- <sup>14</sup> College of Resources and Environment Sciences, Hebei Normal University, Shijiazhuang 050024, China
- <sup>15</sup> Institute of Earth and Environment Science, University of Potsdam, Karl-Liebknecht-Straße 24, 14476 Potsdam, Germany
- <sup>16</sup> Institute of Biochemistry and Biology, University of Potsdam, Karl-Liebknecht-Straße 24, 14476 Potsdam, Germany